

# Experimental investigation of pavement behavior after embankment widening using a fiber optic sensor network

Xiaolin Weng<sup>1</sup>, Hong-Hu Zhu<sup>2</sup>, Jianxun Chen<sup>3</sup>, Dongping Liang<sup>1</sup>, Bin Shi<sup>2</sup> and Cheng-Cheng Zhang<sup>2</sup>

## Abstract

In order to investigate the actual health condition of asphalt concrete pavements on widened road embankments, a full-scale model test study was conducted. A fiber Bragg grating–based sensor network was developed to monitor the strain distributions within the pavement structure, which was subjected to differential settlements. An improved packaging and installation method of the quasi-distributed sensor system was utilized, which not only ensured a high sensor survival rate but also achieved accurate measurement of axial strains in longitudinal and transverse directions. Based on the monitoring results, the strain characteristics of the pavement structure under different settlements were analyzed in detail. It is found that in general, the top layer of the asphalt pavement structure was subject to tension stress due to the differential settlement of the embankment. Plastic deformation of the pavement was observed when the differential settlement increased to 22 cm. The base layer of the pavement had the most significant response in comparison with the top and middle layers. The geogrid reinforcement in the embankment had a positive effect to alleviate the tension stress in the pavement. This experimental study also indicates the capability of fiber optic sensor networks to monitor the performance of pavements with a high degree of accuracy.

## Keywords

Differential settlement, asphalt concrete pavement, embankment, fiber Bragg grating, strain monitoring

## Introduction

With the development of highway transportation, widening or reconstruction of road embankments has been encountered all over the world. The consolidation settlements of old embankments have been completed after several years' operation. When widening of embankment is conducted, the weight of the fill materials will cause additional stresses within the embankment, resulting in new settlements. The differential settlement between the existing and the new embankments may induce unacceptable stresses and deteriorate the working condition of the pavement structure. For instance, longitudinal cracks of the pavement, which are induced by excessive deformation of the embankment, are frequently noticed in widened roads.<sup>1</sup> The vehicle operating and maintenance costs of these poor-quality pavements will be increased considerably. Therefore, it is of great importance to get a better

understanding of the response and performance of the pavement structure due to differential settlement within the widened embankment.<sup>2</sup> However, due to the constraint of testing and measurement techniques, the failure mechanism of pavement of widened road is mainly investigated through small-scale model testing or numerical analysis.<sup>1,3–5</sup>

For pavement structures, geotechnical instrumentation plays an important role in assessing their

<sup>1</sup>Key Laboratory for Special Area Highway Engineering of Ministry of Education, Chang'an University, Xi'an, China

<sup>2</sup>School of Earth Sciences and Engineering, Nanjing University, Nanjing, China

<sup>3</sup>School of Highway, Chang'an University, Xi'an, China

## Corresponding author:

Hong-Hu Zhu, School of Earth Sciences and Engineering, Nanjing University, Nanjing 210046, China.  
Email: zhh@nju.edu.cn

performance. The electric resistance strain gauges, earth pressure cells, soil moisture cells, and accelerometers are commonly utilized for this purpose.<sup>6–12</sup> But these conventional geotechnical instruments are based on point measurement and can only get information from discrete locations on the pavement. The long-term performance of electrical type sensors is suspect because the monitoring data are easily influenced by electrical–magnetic interference (EMI). Furthermore, there are some technical problems encountered during the installation of these sensors.<sup>12</sup> To evaluate the overall performance of pavement structures, a reliable, accurate, and cost-effective distributed sensor network that can get information from multiple points is utterly required.

In the past decade, a series of fiber optic sensing technologies have been developed and applied to health monitoring of various geotechnical-related structures, such as foundations,<sup>13</sup> tunnels,<sup>14,15</sup> caverns,<sup>16</sup> pipelines,<sup>17</sup> and slopes.<sup>18–21</sup> These technologies have shown unique advantages over conventional monitoring methods, including tiny size, high sensitivity, immunity to EMI, good durability, and the ability of multiplexing. The early-stage study on the feasibility of fiber optic sensing in pavement monitoring was introduced by Tang et al.<sup>22</sup> Wang et al.<sup>23</sup> and Wang and Tang<sup>24</sup> developed a high-resolution temperature and strain sensor using fiber Bragg grating (FBG) technology and a simple and low-cost long-period grating (LPG) sensor for measuring the water level in pavement structures. In the research of Dore et al.,<sup>25</sup> the Fabry–Perot (F–P)–based fiber optic strain sensors were applied to monitor small strains of existing pavements. Galal et al.<sup>26</sup> utilized the FBG technology to measure the long-term strain of a pavement under traffic loading during and after construction. Weng and Wang<sup>27</sup> reported the monitoring results of a physical model test of pavement instrumented by horizontally embedded FBG strain sensors. The response of the pavement due to differential settlement of embankment was presented and analyzed. Recently, Zhou et al.<sup>28</sup> utilized the same technology to perform in situ three-dimensional health monitoring of a pavement structure. A number of difficulties have been encountered because Young's moduli of fiber optic sensors are different from those of asphalt concrete pavements. It is shown that there are certain discrepancy between field measurement data of strain distribution and theoretical results.

The primary aim of this study is to characterize the strains of a pavement structure induced by differential settlements of a road embankment after widening. A full-scale model test has been conducted to evaluate the performance of the asphalt concrete pavement. During testing, differential settlements were applied using hydraulic jacks. An FBG-based fiber optic sensor

network was developed and employed to monitor the two-dimensional (2D) strain fields of three layers in the pavement structure. The strain distributions of the pavement are studied in detail.

## FBG-based strain sensor network

The measurement of strains at critical locations in pavement structures is essential for developing and validating pavement theoretical models, based on which rational design and analysis methods of pavements can be obtained. In this study, an FBG-based sensor network was constructed to monitor the strain distribution of the pavement.

The sensing functioning of FBG was first discovered on the formation of photo-generated gratings in germanosilicate optical fiber by Hill et al.<sup>29</sup> The Bragg grating is written into a segment of single-mode fiber, in which a periodic modulation of refractive index in the core of the optical fiber is formed by exposure to a spatial pattern of ultraviolet (UV) light. Figure 1 illustrates the working principle of an FBG sensor. According to Bragg's law, when a broadband source of light interacts with the Bragg grating, a narrow spectral part of light at a certain wavelength is reflected<sup>30</sup>

$$\lambda_B = 2n_{eff}\Lambda \quad (1)$$

where  $\lambda_B$  is called the Bragg wavelength, typically 1510–1590 nm ( $1 \text{ nm} = 10^{-9} \text{ m}$ ),  $n_{eff}$  is the effective refractive index, and  $\Lambda$  is the period of the index modulation.

Through physical or thermal elongation of the sensor segment and through the change in the refractive index of the fiber due to photo-elastic and thermo-optic effect, the Bragg wavelength of an FBG sensor will vary linearly with applied strain or temperature. Considering a standard single-mode silica fiber with the applied strain  $\Delta\varepsilon$  and temperature  $\Delta T$ , this relationship is given by Kersey et al.<sup>31</sup>

$$\frac{\Delta\lambda_B}{\lambda_{B0}} = c_\varepsilon\varepsilon + c_T\Delta T \quad (2)$$

where  $\lambda_{B0}$  is the original Bragg wavelength under strain free and  $0^\circ\text{C}$  condition,  $\Delta\lambda_B$  is the variation in Bragg wavelength due to the applied strain and temperature, and  $c_\varepsilon$  and  $c_T$  are the calibration coefficients of strain and temperature. The typical strain and temperature accuracy of a bare FBG sensor are  $1 \mu\varepsilon$  and  $0.1^\circ\text{C}$ , respectively.

As the FBG sensor is sensitive to both strain and temperature, it is a key problem to separate the effect of temperature from the strain monitoring data in data analysis.<sup>32</sup> This temperature compensation problem can

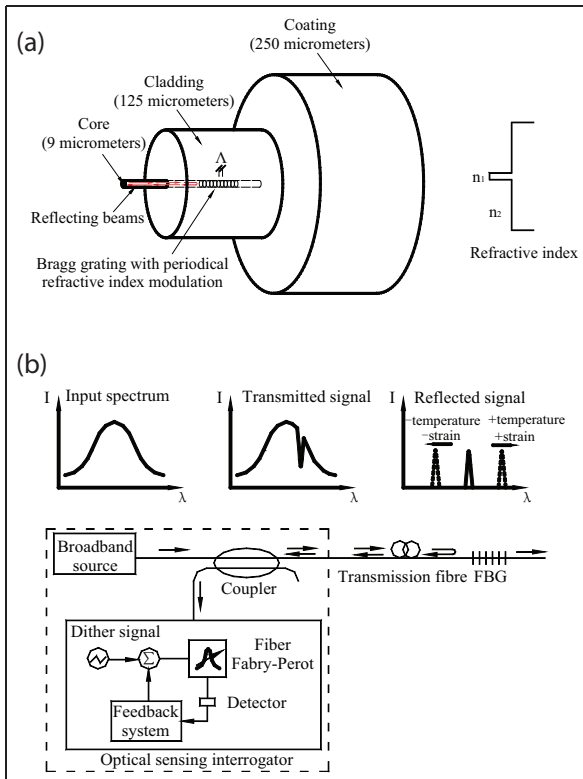


**Figure 1.** Working principle of an FBG sensor: (a) structure of an FBG sensor and (b) strain and temperature sensing of an FBG sensor. FBG: fiber Bragg grating.

be achieved by adding an additional FBG sensor or a conventional temperature sensor to the same temperature field. Once the temperature variation  $\Delta T$  is measured, the mechanical strain can be corrected as follows

$$\Delta \epsilon = \frac{1}{c_\epsilon} \left( \frac{\Delta \lambda_B}{\lambda_B} - c_T \Delta T \right) \quad (3)$$

The advantages of FBG sensors over conventional sensors are shown in Table 1. The FBG sensor can be multiplexed in parallel or in series. Using the technologies of wavelength division multiplexing (WDM) and time division multiplexing (TDM), a number of FBG sensors can form a quasi-distributed sensing array along a single optical fiber, as shown in Figure 2. A sensor network consisting of FBG sensors and interrogators can be easily constructed using a simple configuration.

**Model test to study pavement behavior after widening of embankment**

*Embankment and pavement subsidence simulation system*

The settlement of a road embankment occurs rapidly during construction and shortly after the construction

**Table 1.** Comparison of features of the conventional sensor and the FBG sensor.

Content	Conventional sensor	FBG sensor
Type	Point sensor	Quasi-distributed sensor
Requirement of moisture proof	Yes	No
Data transmission distance	$\leq 100$ m	$\leq 10$ km
Data collection	Manual in most cases	Automatic
Long-term stability	Poor	Good
Price/performance ratio	Poor	Good

FBG: fiber Bragg grating.

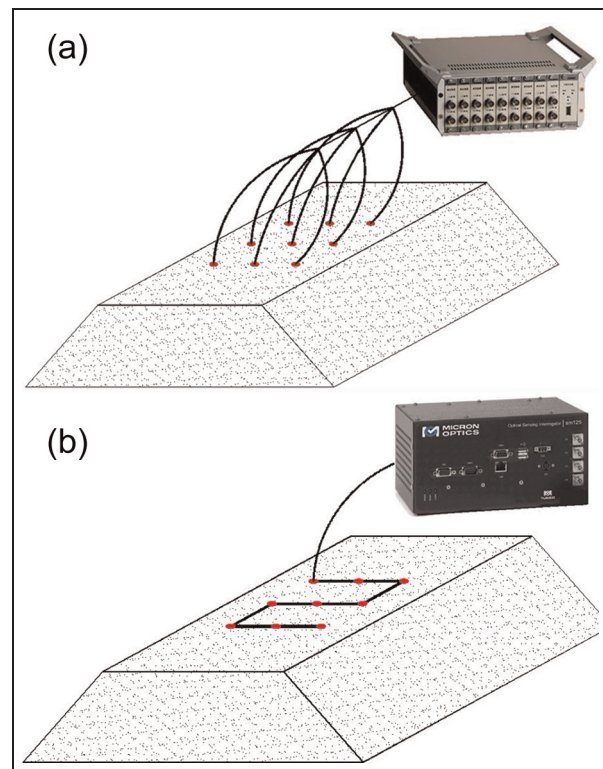


**Figure 2.** Schematic illustration of the difference between conventional and FBG sensors: (a) point measurement sensors and (b) quasi-distributed FBG sensor network.

stage. Subsequently, the consolidation settlement rate of the embankment decreases gradually under its self-weight. Most of the consolidation settlement has been completed when the highway has been opened for a period of time, for example, 1 or 2 years. Therefore, the differential settlement due to the widening of road embankment dominates the overall deformation of road embankment.

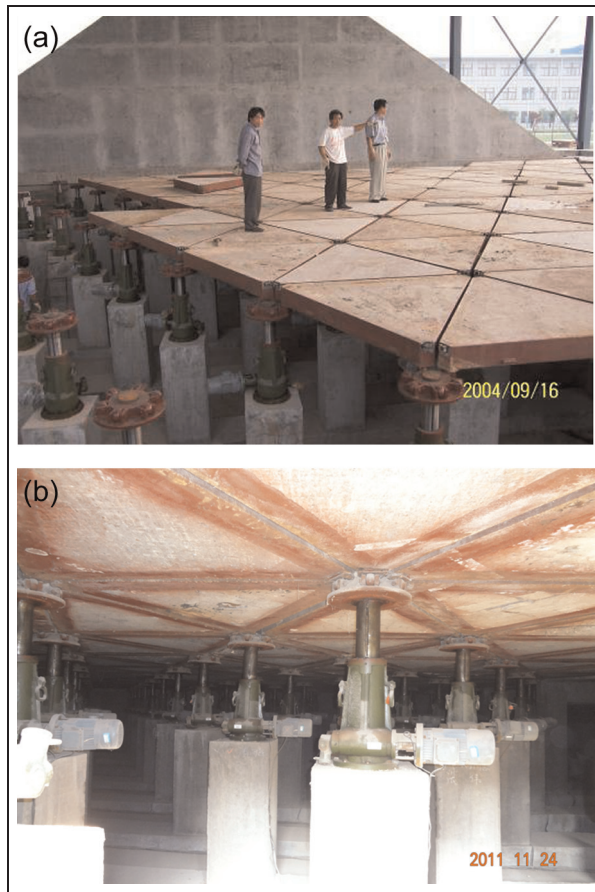


**Figure 3.** Photograph of the embankment and pavement subsidence simulation system: (a) close-up view of the test rig panels and (b) close-up view of the hydraulic jacks.

To study the pavement behavior after the widening of embankment, a model test was conducted using the large-scale embankment and pavement subsidence simulation system in Chang'an University, China, as shown in Figure 3. This test system includes the following parts: (a) ground support and lifting subsystem, (b) measurement subsystem, and (c) servo-load controlling subsystem. There are 230 pieces of equilateral triangle panels in the ground support subsystem. At the vertex of six adjacent panels, there is a self-lock hydraulic jack with a capacity of 100 ton and a load cell that is used to measure its load. The block test rig panels are assembled to form the ground surface. The translation and rotation of the test rig panels can be controlled freely, and thus, different types of settlement pattern and settlement rate of embankment can be approximately simulated.

### *Model test of the widened embankment*

In the model test of the widened embankment, at the centerline of the old embankment, a rigid reinforced concrete wall was set as the left boundary as this is a symmetrical problem. The old pavement that had a

half-width of 6 m was designed to be widened to 10 m, as shown in Figure 4. The longitudinal length of the embankment was 10 m. To evaluate the contribution of geogrids embedded in the embankment to enhancing the performance of the pavement, half of the embankment was reinforced by two layers of geogrids. One layer was placed under the very bottom of the model embankment and the other was under the lime-stabilized layer. The dimensions of the geogrids are shown in Figure 5.

By adjusting the vertical lifting displacements of hydraulic jacks at different locations, predefined differential settlements of the widened embankment were applied. According to typical settlement characteristics of widened embankments,<sup>1</sup> it is assumed that the maximum settlement  $S_2$  occurs at the road shoulder of the widened road and the minimum settlement  $S_1$  occurs at the centerline of the old road embankment. The differential settlements between the old and new embankments are defined as  $S = S_2 - S_1$ . In this experimental study,  $S$  increased from 2 to 22 cm in stages (see Figure 6), so that the effect of the differential settlement on the pavement response can be investigated.

The subgrade soil of the road embankment is loess taken from a road construction site in Xi'an, China. Table 2 presents the physical and mechanical properties of the soil. According to the laboratory compaction tests, the optimum moisture content  $w_{opt}$  of the soil is 13.2%. To simulate the difference of stiffness between the old and new embankments, the fill material of the old embankment was mixed with lime with a weight ratio of 4%. The moisture content and density were strictly controlled during the construction process of the embankment, which is essential for attaining a uniformly dense and stable embankment. The soils were placed at a moisture content within  $\pm 1\%$  of the optimum and a relative density of over 98% was achieved after compaction. After the construction stage, the average moisture content and the dry density of the soil were measured to be 13.3% and  $1.90 \text{ g/cm}^3$ , respectively.

A 54-cm-thick layer of semi-rigid cement-stabilized crushed-stone base course was placed on the embankment, as shown in Figure 4. The cement-stabilized crushed-stone base materials with weight ratios of 4%, 5%, and 6% were mixed manually and compacted in three 18-cm-thick sub-layers using a 12-ton road roller. The average unconfined compressive strength of the test samples was measured to be 4.2 MPa, which is greater than the minimum required strength of 4.0 MPa. A series of standard compaction tests were conducted on the cement-stabilized crushed-stone with the moisture content of 4%, 5%, 6%, 7%, and 8%, respectively. The maximum dry density and the optimum moisture content were  $2.32 \text{ g/cm}^3$  and 5.5%, respectively.

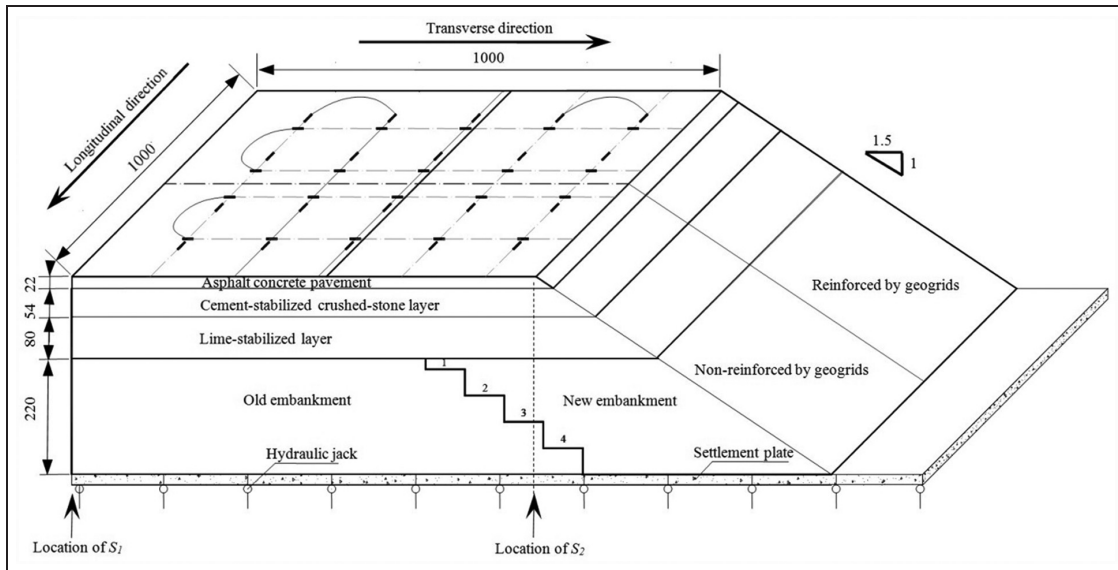


Figure 4. Physical model of a widened road embankment instrumented with the fiber optic sensor network (cm).

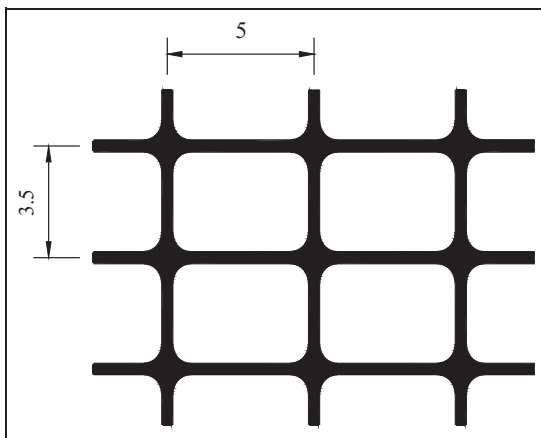


Figure 5. Dimensions of the geogrids used in the embankment (cm).

The asphalt concrete pavement also consisted of three layers and their thicknesses, from top to bottom, are 4, 6, and 12 cm, respectively. The asphalt concrete pavement was made of AC-13 asphalt mixture. The drill core sample test results show that the construction had a degree of compaction over 95%, which met the pavement construction specifications of China.

*Instrumentation of the model pavement*

The strains of the asphalt pavement in this full-scale model test were monitored by an FBG sensor network. However, the optical fiber itself is very thin and has limited tension and shear resistance. During the construction process, the sensor is very easy to damage or break, which makes the installation quite difficult. It is thus of great importance to develop a sensor protection

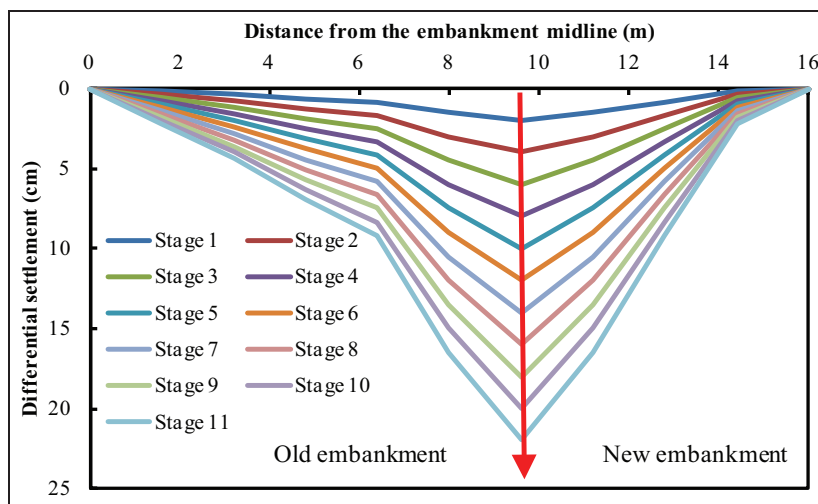
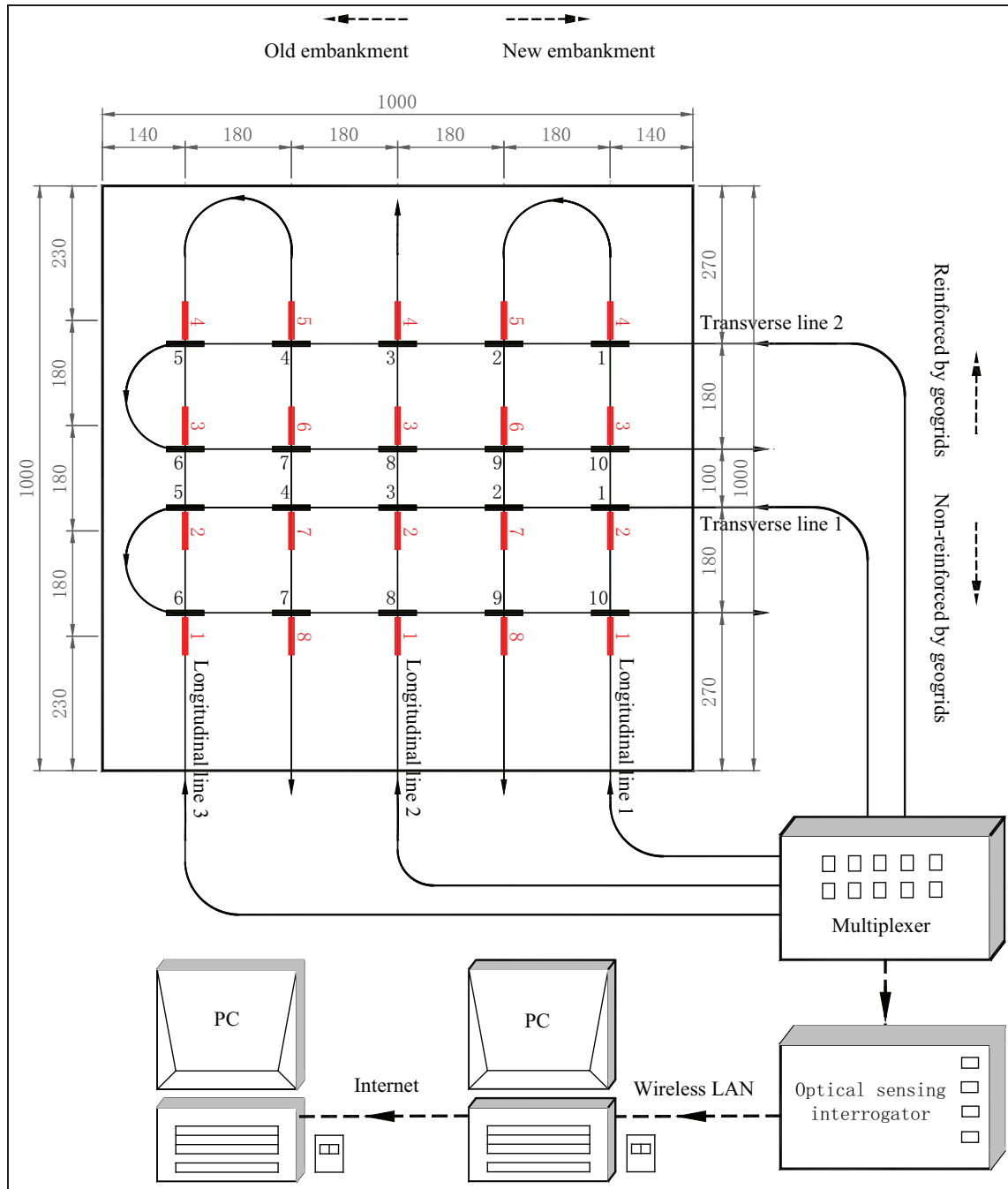


Figure 6. Settlement profile applied on the road embankment.



**Figure 7.** Layout of the FBG sensor network to measure the strains of the pavement (cm).

system to ensure not only the survival ratio of the FBG sensors but also the reliability of observational data.

The three asphalt concrete layers were instrumented with both longitudinal and transverse FBG strain sensors, as shown in Figure 7. For each layer, there were four transverse monitoring sections and five longitudinal monitoring sections. A tube-packaged FBG temperature sensor was embedded in the pavement for temperature compensation. Using linear interpolation,

2D strain distributions of the pavement can be obtained.

To install the fiber optic sensor network, a 5 mm × 5 mm groove was prepared on every pavement layer using a cutting machine. An air compressor was utilized to clean the grooves by compressed air. Afterward, the armored optical cables containing FBG sensors were placed into the grooves. In order to make the FBG sensors in close contact with the asphalt pavement, the

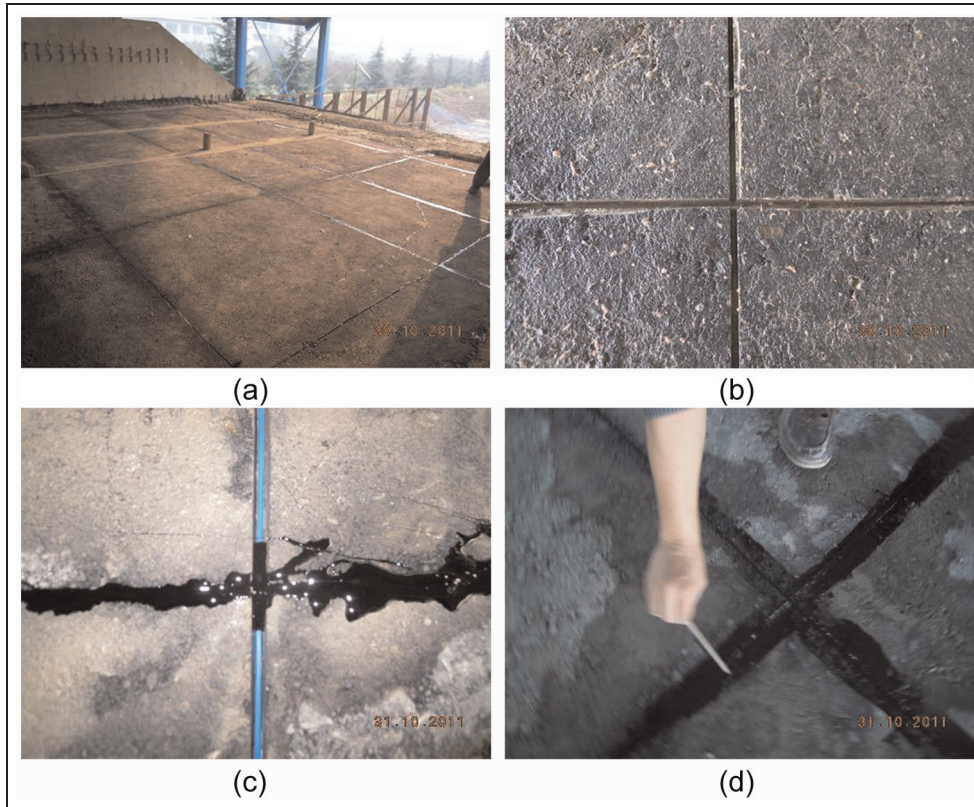


**Figure 8.** Photographs of the installation of the fiber optic sensor network: (a) location of the sensor network, (b) preparation of the groove, (c) embedded optical fiber cable, and (d) filling the grooves with asphalt.

**Table 2.** Physical and mechanical properties of the subgrade soil.

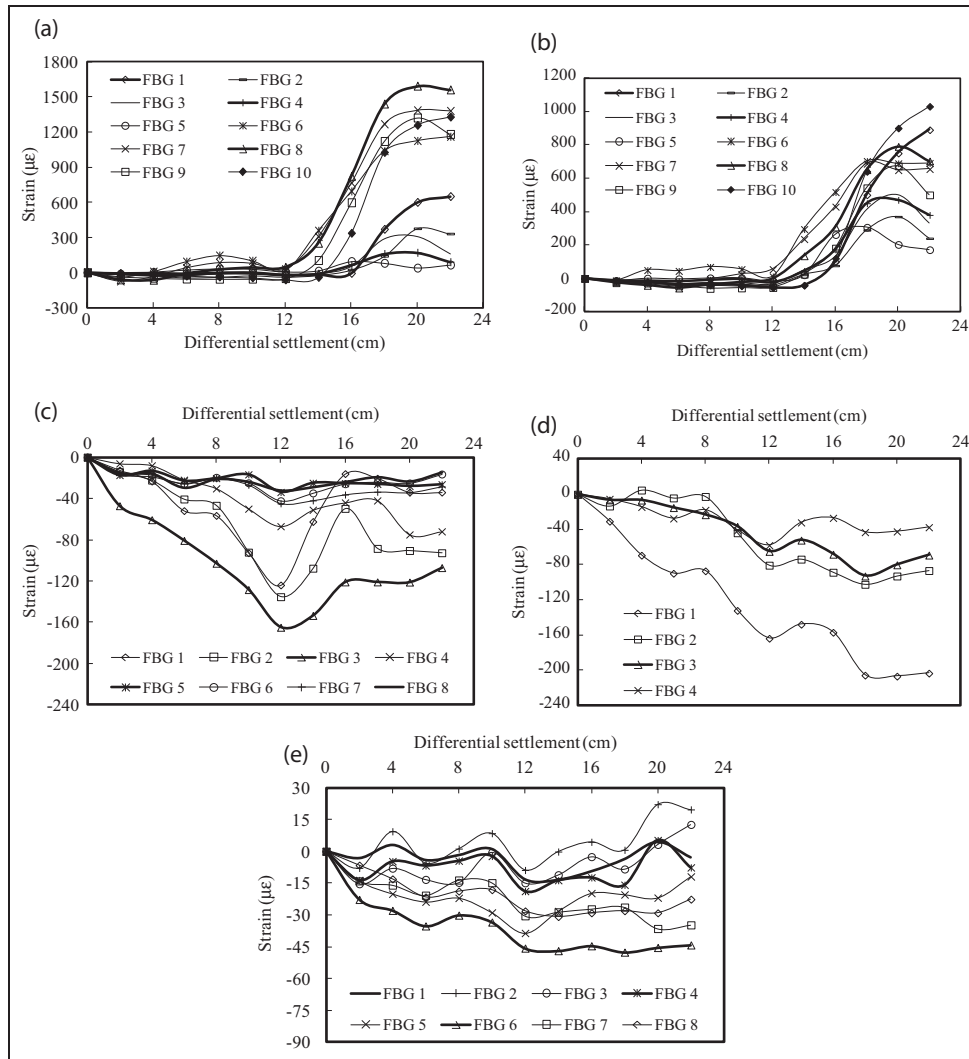
Moist density $\rho$ (g/cm <sup>3</sup> )	Void ratio $e$	Water content $w$ (%)	Degree of saturation $S_r$ (%)	Poisson's ratio $\nu$	Cohesion $c$ (kPa)	Friction angle $\varphi$ (°)
2.15	0.63	12.56	38.6	0.37	21.75	22.58

sensors were embedded by a mixture of hot asphalt and gasoline. Laboratory trial tests show that after gasoline evaporation, the mechanical properties of the remaining asphalt were very close to the pavement material. This method can guarantee that the observed strains were real strains of the pavement. Figure 8 shows the close-up view of the sensor installation procedure. Before differential settlements were applied, the FBG signals were checked and only two sensors in the longitudinal lines were broken, which means that a sensor survival ratio of 98.3% was achieved.

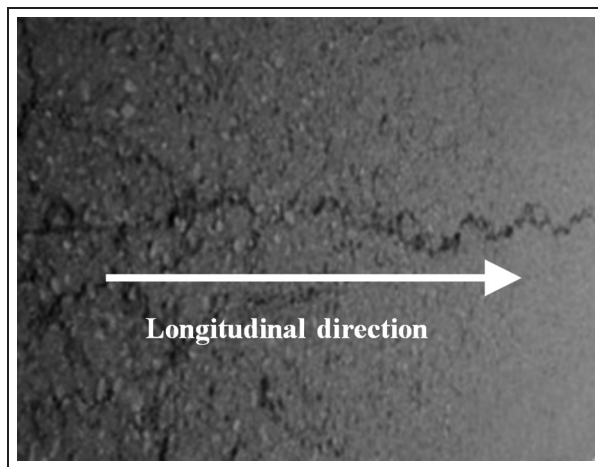
### Test results and analysis

Figure 9 presents the variations in strain at the top layer of the asphalt concrete pavement. It is found that

under the influence of differential settlement, the pavement surface was subjected to tension loads in general. With the increase of differential settlement, the transverse strains increased gradually but remained at a low level. When  $S$  reached 14 cm, the strains began to rise sharply, indicating plastic response of the pavement structure. This phenomenon shows that the differential settlement induced large additional stresses in the pavement, which is consistent with other studies.<sup>26</sup> When  $S$  increased to 20–22 cm, the readings of all the FBG sensors peaked. Eventually, a number of small cracks on the pavement, mostly in the longitudinal direction, were observed, as shown in Figure 10. These cracks demonstrate that the transverse strains in the pavement were accumulated to a high magnitude and localized tension failure occurred.



**Figure 9.** Transverse and longitudinal strains of the top layer of the asphalt concrete pavement: (a) transverse line 1, (b) transverse line 2, (c) longitudinal line 1, (d) longitudinal line 2, and (e) longitudinal line 3. FBG: fiber Bragg grating.



**Figure 10.** Observed cracks on the pavement after the test.

The longitudinal strains of the pavement are shown in Figures 9(c) to (e). The top layer of the pavement was in the state of compression due to the differential settlement. Because longitudinal line 2 was close to the joint zone of old and new embankments and influenced by non-uniform deformation, its strains were larger than those of the other two lines. The comparison of transverse and longitudinal strains shows that the magnitudes of strain in these two directions were quite different. This may result from the anisotropic boundary conditions and the anisotropic behavior of the model embankment. The uneven settlement of the new embankment should also contribute to this phenomenon.

Figure 11 shows the strains of the middle and base layers. It is found that the relationships between strain

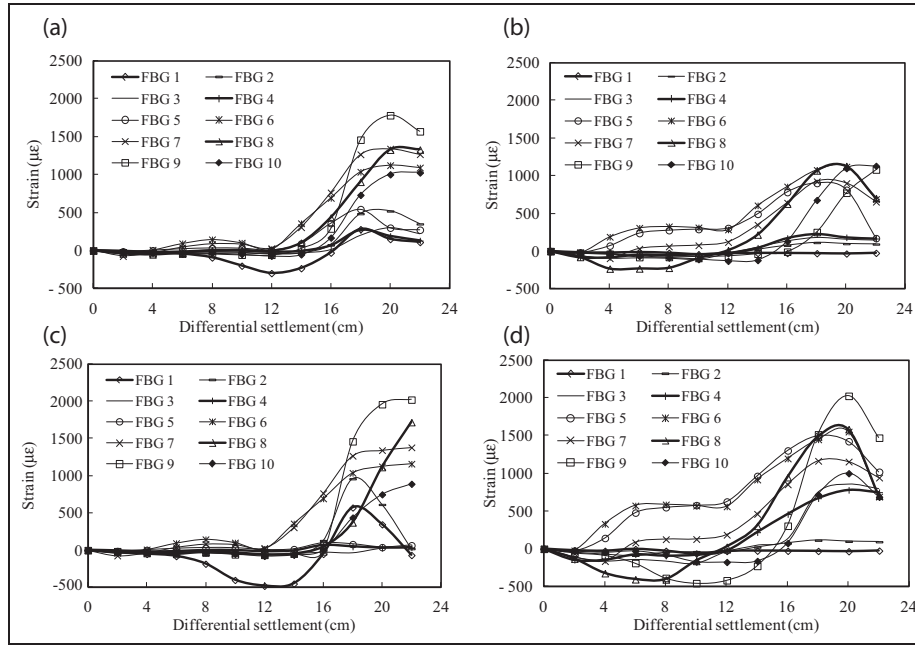


**Figure 11.** Transverse strains measured by the FBG sensors in the middle and base layers: (a) transverse line 1 in the middle layer, (b) transverse line 2 in the middle layer, (c) transverse line 1 in the base layer, and (d) transverse line 2 in the base layer. FBG: fiber Bragg grating.

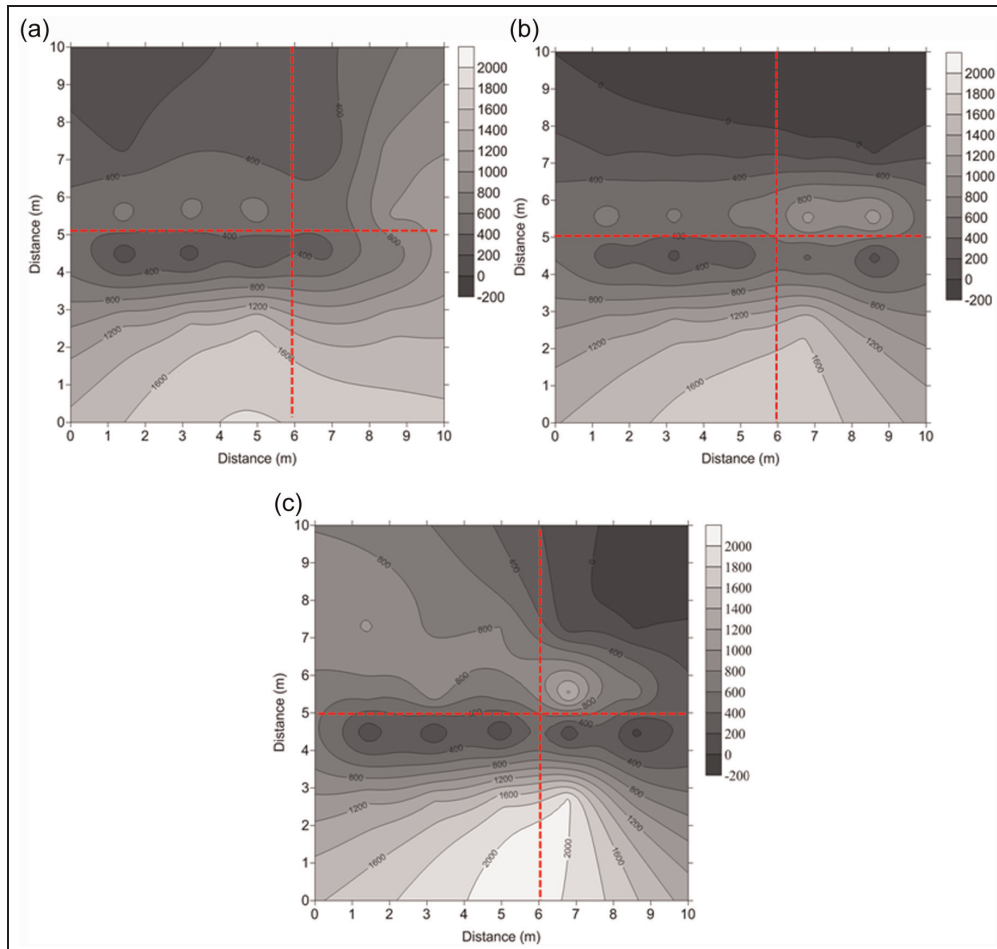


**Figure 12.** Distributions of measured transverse strains in the pavement layers: (a) top layer, (b) middle layer, and (c) base layer.

and differential settlement were similar to those of the top layer. Under the same settlement condition, the strains of the base layer were the largest among all the pavement layers.

The distributions of transverse strain of all the three layers when the differential settlement reached 22 cm are shown in Figure 12. Under the same magnitude of differential settlement, the strain measurements of the pavement layers on the geogrid reinforced embankment were smaller than those on the embankment without geogrids. This indicates that the geogrids can effectively enhance the structural integrity of the pavement and embankment system, which is consistent with the observations of Zhang et al.<sup>5</sup>

## Conclusion

In this article, a preliminary attempt is introduced to apply the FBG sensor network to evaluating the performance of a pavement after embankment widening. The working principle, design, and installation method are presented in detail. A full-scale model test was conducted to study the response of pavements under differential settlements, and the strain monitoring results from the FBG sensors are analyzed. From this experimental study, the following conclusions are drawn:

1. The asphalt pavement structure after embankment widening is subject to tension stresses in general, which are induced by differential settlements of the road embankment. The accumulated transverse strains may result in tension cracks of the pavement.
2. The strains of the base layer of the pavement are considerably larger than those of the middle and top layers.
3. The geogrid reinforcement can effectively enhance the structural integrity of the pavement.
4. It is verified that the fiber optic sensor network is able to monitor the strains of the pavement with a high degree of accuracy.

## Funding

This work was supported by the National Natural Science Foundation of China (grant nos 41302217, 51008032, and 51378004) and the National Basic Research Program of China (973 Program) (grant no. 2011CB710605).

## References

1. Han J, Oztoprak S, Parsons RL, et al. Numerical analysis of foundation columns to support widening of embankments. *Comput Geotech* 2007; 34(6): 435–448.
2. Deschamps RJ, Hynes CS and Bourdeau PL. Embankment widening design guidelines and construction procedures. Report, Indiana Department of Transportation and Purdue University, West Lafayette, IN, September 1999.
3. Wang H and Huang XM. Centrifuge model test and numerical analysis of embankment widening on soft ground. In: *Proceedings of the eighth international conference on applications of advanced technologies in transportation engineering*, Beijing, China, 26–28 May 2004, pp. 548–553. Reston, VA: American Society of Civil Engineers (ASCE).
4. Chen YK, Wang YM and Ren C. Analysis of the influence of embankment widening on soft ground with differential settlements on pavement structure. In: *Proceedings of the GeoShanghai international conference 2010*, Shanghai, China, 3–5 June 2010, pp. 239–248. Reston, VA: American Society of Civil Engineers (ASCE).
5. Zhang JH, Zheng JL and Huang XM. Centrifuge model test and numerical analysis of geosynthetic-reinforced embankments for a road widening. In: *Proceedings of the GeoHunan international conference 2011*, Hunan, China, 9–11 June 2011, pp. 204–210. Reston, VA: American Society of Civil Engineers (ASCE).
6. Brandon TL, Al-Qadi IL, Lacina BA, et al. Construction and instrumentation of geosynthetically stabilized secondary road test sections. *Transport Res Rec* 1996; 1534: 50–57.
7. Zafar R, Nassar W and Elbella A. Interaction between pavement instrumentation and hot mix asphalt in flexible pavement. *Emir J Eng Res* 2005; 10(1): 49–55.
8. Ryden N and Lowe MJS. Guided wave propagation in three-layer pavement structures. *J Acoust Soc Am* 2004; 116(5): 2902–2913.
9. Rynnänen T, Pellinen T and Belt J. The use of accelerometers in the pavement performance monitoring and analysis. *IOP Conf Ser: Mater Sci Eng* 2010; 10(1): 1–10.
10. Gonçalves PF, Ceratti JAP and Bica AVD. The use of embedded stress cells for monitoring pavement performance. *Geotech Test J* 2003; 26(4): 363–372.
11. Seo Y. A full scale in situ evaluation of strain characteristics at highway flexible pavement sections. *J Test Eval* 2010; 38(4): 390–399.
12. Seo Y and Lee JH. Short- and long-term evaluation of asphalt concrete strain gauge installation methods applied to the KHCTR. *J Transp Eng* 2012; 138(6): 690–699.
13. Lee W, Lee WJ, Lee SB, et al. Measurement of pile load-transfer using the fiber Bragg grating sensor system. *Can Geotech J* 2004; 41(6): 1222–1232.
14. Metje N, Chapman DN, Rogers CDF, et al. An optical fiber sensor system for remote displacement monitoring of structures—prototype tests in the laboratory. *Struct Health Monit* 2008; 7(1): 51–63.
15. Li C, Zhao Y, Liu H, et al. Combined interrogation using an encapsulated FBG sensor and a distributed Brillouin tight buffered fiber sensor in a tunnel. *Struct Health Monit* 2010; 9(4): 341–346.
16. Zhu WS, Zhang QB, Zhu HH, et al. Large-scale geomechanical model testing of an underground cavern group in a true three-dimensional (3-D) stress state. *Can Geotech J* 2010; 47(9): 935–946.

17. Glisic B and Yao Y. Fiber optic method for health assessment of pipelines subjected to earthquake-induced ground movement. *Struct Health Monit* 2012; 11(6): 696–711.
18. Wang BJ, Li K, Shi B, et al. Test on application of distributed fiber optic sensing technique into soil slope monitoring. *Landslides* 2009; 6(1): 61–68.
19. Pei HF, Cui P, Yin JH, et al. Monitoring and warning of landslides and debris flows using an optical fiber sensor technology. *J Mt Sci-Engl* 2011; 8(5): 728–738.
20. Zhu HH, Ho ANL, Yin JH, et al. An optical fiber monitoring system for evaluating the performance of a soil nailed slope. *Smart Struct Syst* 2012; 9(5): 393–410.
21. Zhu HH, Shi B, Zhang J, et al. Distributed fiber optic monitoring and stability analysis of a model slope under surcharge loading. *J Mt Sci-Engl* 2014; 11(4): 979–989.
22. Tang JL, Wang JN, Chien EL, et al. Use of fiber Bragg grating sensors for fiber optic pavement monitoring system development. In: *Proceedings of the 5th pacific rim conference on lasers and electro-optics*, Taipei, China, 15–19 December 2003, p. 571. Piscataway, NJ: Institute for Electrical and Electronic Engineers (IEEE).
23. Wang JN, Tang JL and Chang HP. Fiber Bragg grating sensors for use in pavement structural strain temperature monitoring. In: *Proceedings of the SPIE, smart structures and materials*, San Diego, CA, 26 February 2006, pp. 1205–1216. Bellingham, WA: SPIE.
24. Wang JN and Tang JL. Optical fiber grating-based sensing system for use in pavement health monitoring. In: *Proceedings of the SPIE, sensors and smart structures technologies for civil, mechanical, and aerospace systems*, San Diego, CA, 9–13 March 2008, pp. 1–11. Bellingham, WA: SPIE.
25. Dore G, Duplain G and Pierre P. Monitoring mechanical response of in service pavements using retrofitted fiber optic sensors. In: *Proceedings of the advanced characterizations of pavement and soil engineering materials*, Athens, 20–22 June 2007, pp. 883–891.
26. Galal KA, Sharp SR and Elfino MK. Fiber-optic sensors strain measurements under an asphalt layer during and after construction. In: *Proceedings of the transportation research board 86th annual meeting*, Washington, DC, 21–25 January 2007. Washington, DC: Transportation Research Board (TRB).
27. Weng XL and Wang W. Influence of differential settlement on pavement structure of widened roads based on large-scale model test. *J Rock Mech Geotech Eng* 2011; 3(1): 90–96.
28. Zhou Z, Liu WQ, Huang Y, et al. Optical fiber Bragg grating sensor assembly for 3D strain monitoring and its case study in highway pavement. *Mech Syst Signal Pr* 2012; 28(S1): 36–49.
29. Hill KO, Malo B, Bilodeau F, et al. Bragg gratings fabricated in monomode photosensitive optical fiber by UV exposure through a phase mask. *Appl Phys Lett* 1993; 62(10): 1035–1037.
30. Morey WW, Meltz G and Glenn WHG. Fiber optic Bragg grating sensors. In: *Proceedings of the SPIE, fiber optic and laser sensors*, Boston, MA, 13 February 1990, pp. 98–107. Bellingham, WA: SPIE.
31. Kersey AD, Davis MA, Patrick HJ, et al. Fiber grating sensors. *J Lightwave Technol* 1997; 15(8): 1442–1463.
32. Guo ZS. Strain and temperature monitoring of asymmetric composite laminate using FBG hybrid sensors. *Struct Health Monit* 2007; 6(3): 191–197.